Molecular Neurobiology (2023) 60:3824–3838
https://doi.org/10.1007/s12035-023-03318-7

miR-671-5p Upregulation Attenuates Blood–Brain Barrier Disruption in the Ischemia Stroke Model Via the NF-κB/MMP-9 Signaling Pathway

Ling Deng[1] · Jiyu Zhang[2] · Sha Chen[1] · Yu Wu[1] · Xiaomei Fan[1] · Tianrui Zuo[1] · Qingwen Hu[1] · Lu Jiang[1] · Shaonan Yang[1] · Zhi Dong[1]

Received: 6 September 2022 / Accepted: 14 March 2023 / Published online: 22 March 2023

Abstract

Blood-brain barrier (BBB) disruption can induce further hemorrhagic transformation in ischemic stroke (IS). miR-671-5p, a micro-RNA, is abundant in the cortex of mammalian brains. Herein, we investigated the roles and potential mechanisms for the effects of miR-671-5p on BBB permeability in IS. Results showed that miR-671-5p levels were significantly downregulated in the cerebral cortex of middle cerebral artery occlusion/reperfusion (MCAO/R) C57/BL6 mice *in vivo*. miR-671-5p agomir administration via right intracerebroventricular injection significantly reduced infarct volume, improved neurological deficits, the axon of neurons and nerve fiber, attenuated cell injury and apoptosis, as well as reduced BBB permeability in MCAO/R mice. Treatment with miR-671-5p agomir alleviated tight junction proteins degradation, including claudin, occludin, and ZO-1 in MCAO/R mice, and these effects were reversed following NF-κB overexpression. Bend.3 brain endothelial cells were subjected to oxygen and glucose deprivation/reoxygenation (OGD/R) treatment *in vivo*, and then miR-671-5p agomir was transfected into the cells. This resulted in reduction of cytotoxicity, improved cell viability, trans-endothelial electrical resistance, reduced fluorescein sodium permeability, and inhibited tight junction degradation in Bend.3 OGD/R cells. However, these effects were reversed following NF-κB overexpression. These results demonstrated that upregulation of miR-671-5p in IS models *in vivo* and i*n vitro* alleviated BBB permeability by targeting NF-κB/MMP-9. In summary, miR-671-5p is a potential therapeutic target for protecting BBB permeability in IS to minimize cerebral hemorrhage transformation.

Keywords Ischemia stroke · Blood–brain barrier · miR-671-5p · NF-κB · tight junction

Introduction

Stroke refers to the loss of neurological functions caused by sudden obstruction of blood supply due to thrombosis or embolism in the cerebra, resulting in cerebral ischemia and hypoxia which further cause cerebral injuries [1–3]. Stroke is a life-threatening disease associated with high morbidity, mortality, and disability rates [4]. Intravenous thrombolysis using recombinant tissue-type plasminogen activator (RT-PA) is recommended for IS. However, this method has a narrow therapeutic time window (< 4.5 h) and high risk of hemorrhagic transformation [1]. Therefore, there is a need to identify novel treatments for IS that do not increases the risk of hemorrhagic transformation.

The blood-brain barrier (BBB) is an important physical barrier that modulates cerebral homeostasis and protects the brain tissue from exposure to potentially hazardous substances [5]. After IS, pathophysiological changes trigger BBB disruption, further causing life-threatening edema and hemorrhagic transformation [6]. Brain hemorrhage is a significant manifestation of BBB destruction, and a severe complication of RT-PA in IS treatment [7].

MicroRNAs (miRNAs) are small endogenous RNAs with a length of fewer than 25 nucleotides involved in the regulation of gene expression. Non-coding RNAs are also involved in the transcriptional and post-transcriptional regulation of genes [8, 9]. Reports indicate that miRNAs mediate

✉ Zhi Dong
100798@cqmu.edu.cn

[1] College of Pharmacology, The Key Laboratory of Biochemistry and Molecular Pharmacology, Chongqing Medical University, Chongqing 400016, China

[2] Pain Department, Traditional Chinese Medicine Hospital of Jiulongpo District in Chongqing, Chongqing 400050, China

the pathological processes of IS [10–12]. miR-671 is highly abundant in mammalian brain regions, including the cortex, hippocampus, cerebellum, and olfactory bulbs; moreover, it binds to circular RNA (circRNA) Cdr1, to regulate neuronal activities in human and mouse brains [13, 14]. miR-671-5p inhibits osteosarcoma development by downregulating TUFT1 levels [15]. It also potentially prevents tumor migration and cancer stem cell characteristics by inhibiting the post-transcriptional activities of TRAF2 [16].

Tight junctions (TJs), including occludin, claudins, and zonula occludens (ZO-1, ZO-2, ZO-3) between endothelial cells are important components of the BBB. The integrity of TJs is lost after stroke, which may improve paracellular permeability, thereby promoting edema and hemorrhagic transformation [17]. Matrix metalloproteinase-9 (MMP-9) is activated during IS, leading to the induction of BBB disruption and TJs degradation [18]. MMP-9 expression are regulated by NF-κB, which is involved in inflammation [19, 20]. NF-κB is a target of miR-671-5p by dual luciferase reporter assay [21]. In this study, we evaluated the roles and potential mechanisms of miR-671-5p on BBB permeability in IS.

We hypothesized that upregulation of miR-671-5p can attenuate TJ-loss-induced permeability of the BBB in ischemia by targeting NF-κB/MMP-9.

Materials and Methods

Establishment of the MCAO/R Model

Male C57BL/6 mice (8–10 weeks old, 20-25 g) were kept at the Animal Experiment Center of Chongqing Medical University with free access to food and water, in a room with a 12 h light/dark cycle, 25 °C ± 2 °C temperature, and 60% – 70% relative humidity. All animal operation procedures were approved by The Institutional Animal Ethics Committee of Chongqing Medical University. Animal suffering was minimized whenever possible.

Before surgery, mice were subjected to fasting for 12 h but were allowed free access to drinking water. The MCAO/R surgery was performed as described in previously documented protocols [22]. Mice were intraperitoneally anesthetized with pentobarbital sodium (40 mg/kg, Sunlidabio, Nanjing, China) and fixed on supine position. Subsequently, their right common carotid arteries (CCA), right internal carotid arteries (ICA), and right external carotid arteries (ECA) were surgically exposed. Further, the ECA was ligated and a silicone nylon monofilament suture (0.21 mm in diameter; Fengteng Biology, Xi'an, China) with a blunted tip coated gently inserted from CCA into ICA until occlusion of the middle cerebral artery for 60 min, approximately 12.0 mm from the distal bifurcation of the carotid artery. The sham group mice were subjected to the same surgical procedures as MCAO mice, except that nylon filaments were not inserted.

Mice with neurological deficit score greater than 1 were evaluated for MCAO success based on a modified version of Bederson's method [23]. Neurological deficit scores of mice were blinded as follows: mice tails were suspended to assess forelimb flexions. 0 score, mice were actively normal, without neurological dysfunctions; 1 score, mice did not fully extend their left forelimbs when excluded; 2 scores, mice were unable to extend their contralateral forelimbs; 3 scores, mice unilaterally rotated when walking freely; 4 scores, mice could not spontaneously walk; 5 scores, mice were rolling to the contralateral side or death.

Experimental Protocol

Experimental protocols for both *in vitro* and *in vivo* assays are provided in Fig. S1 in Additional File 1. The miR-671-5p agomir and miR-671-5p antagomir were bought from Sagon Biotech, Shanghai, China. Plasmid pcDNA3.1 NF-κB was bought from GenePharma, Shanghai, China. Vectors or plasmids were transfected into Bend.3 cells using the riboFECT CP reagent (RIBBIO, Guangzhou, China). Next, the cells were subjected to OGD/R treatment and cultured under normal conditions for 24 h.

Right intracerebroventricular injection protocol: Mice were anesthetized through intraperitoneal administration of pentobarbital sodium and laced on a stereotaxic apparatus (San Diego, USA) in prone positions. The miR-671-5p agomir, miR-671-5p antagomir, and plasmid pcDNA3.1 NF-κB were injected into the right lateral ventricle (1.0 mm right lateral, 0.5 mm posterior, and 3.0 mm below the horizontal plane of the bregma) [24] using a 5 μL mini-pump syringe (RWD, Ningbo, China).

Fluorescence in Situ Hybridization (FISH)

The miR-671-5p probe signals were detected using the Fluorescent *in Situ* Hybridization Kit (Sagon Biotech, Shanghai, China), following the manufacturer's instructions. The sequence of the mir-671-5p probe was -DIG-CTCCAGCCC CTCCAGGG.

CTTCCT-3'. Platelet endothelial cell adhesion molecule-1 (PECAM-1; CD31, Servicebio, Wuhan, China), Glial fibrillary acidic protein (GFAP, Servicebio, Wuhan, China), and Neuronal nuclei (Neun, Servicebio, Wuhan, China) were used to label brain microvascular endothelial cells (BMVEC), astrocytes, and neurons of mice cortex by immunofluorescent staining. 4, ′6-diamidino-2-phenylindole (DAPI) was used to stain the cell nucleus. The cells were imaged using a fluorescence microscope (Nikon, Tokyo, Japan).

High-throughput RNA Sequencing Data Analysis

Total RNA was extracted from mice brains using the Trizol reagent (Sagon Biotech, Shanghai, China), following the manufacturer's instructions. Thereafter, the RNA quality was evaluated using the Qubit RNA detection Kit (Life, Q32855). High-throughput RNA sequencing was conducted by Illumina Nexseq500 SE75 (Illumina, San Diego, CA, USA) to sequence the miRNA library. Genes were considered to be significantly differentially expressed between sham and MCAO/R groups when $p < 0.05$ and fold change cutoff as $|\log2 \text{ ratio}| \geq 0.5$. A heatmap of 30 miRNAs was plotted using Multi Experiment Viewer 4.9.0 software.

Rota-rod Test

Coordination and fatigue resistance in mice were evaluated using a Rota-rod cylinder (Ugo Basile, Italy). Before MCAO surgery, all mice were subjected to single baseline test training. Mice that could last for 160 s on the Rota-rod cylinder as the speed slowly increased from 4 to 40 rpm within 5 min were selected for further experiments. At 24 h after MCAO, the fall latency time of mice was recorded under similar training speeds.

Measurement of the Infarct Area

At 24 h after MCAO/R surgery, mice brains were harvested, sliced into coronal sections, and stained using 2% 2,3,5-triphenyl tetrazolium chloride (TTC, Sigma, St Louis, MO, USA) for 15 min at 37 °C. The infarcted area of the brain appeared white, whereas the other area was red. The infracted area was detected using ImageJ, and the proportion of infracted area to the total area was determined as follows: infarct area (%) = (infarct area – [ipsilateral hemisphere area – intact contralateral hemisphere area]) × 100/ intact contralateral hemisphere area [21].

Hematoxylin and Eosin (H&E) Staining

At 24 h after MCAO/R surgery, mice were anesthetized and transcardially perfused with heparinized saline and 4% paraformaldehyde (Servicebio, Wuhan, China). The whole brain was obtained, embedded in paraffin wax, sliced into coronal sections, stained with H&E staining, and imaged by light microscopy (Nikon, Tokyo, Japan). Percentage of injured cells (%) = injured cell counts × 100/total cell counts [25].

Glycine Silver Staining

Axonal degeneration was evaluated through glycine silver staining [26]. The sliced sections were dewaxed and rehydrated with xylol I for 20 min, xylol I for 20 min, ethyl alcohol for 15 min, 75% ethyl alcohol for 5 min, and washed using ddH_2O. Subsequently, the sections were orderly treated with glycine silver stain C, glycine silver stain B, and glycine silver stain A (G1052, Servicebio, Wuhan, China) in line with the manufacturer's protocol. Thereafter, the sections were dehydrated and sealed with a sheet soaked in ethyl alcohol and xylol and then imaged under a light microscope (Nikon, Tokyo, Japan).

Evans Blue Extravasation

The integrity of blood-brain barrier permeability was evaluated using the Evans blue extravasation as previously reported [27]. At 24 h after MCAO, 2% Evans blue (4 ml/kg, Xiya Chemical Industries, Shandong) was administered to every group of mice via intravenous injection through the tail. After 3 h, animals were euthanized and perfused with PBS. The right hemispheres were collected and homogenized in 50% trichloroacetic acid. The homogenate was centrifuged at 12,000 rpm, and 4 °C for 15 min. Then, the supernatant was double diluted with ethanol overnight at 4 °C in the dark. Evans blue concentration in the supernatant was quantitatively determined using a fluorescence plate reader (Thermo Scientific, USA) at an absorbance of 610 nm. The results are recorded as (μg of Evans blue leakage)/ (g of tissue).

The Terminal Deoxynucleotidyl Transferase dUTP Nick End Labeling (TUNEL) Staining

TUNEL staining (G1051, Servicebio, Wuhan, China) was performed to detect cell apoptosis based on the instructions. Briefly, the paraffin-embedded samples were incubated with proteinase K (G1234-1ML, Servicebio, Wuhan, China) solution at 37 °C for 30 min and 2 rinses with PBS. Triton 0.1% (G1204-100ML, Servicebio, Wuhan, China) solution was added, incubated for 30 min at 37 °C, and washed twice with PBS. DAPI was added, incubated for 10 min, dropwise added glycerol, cover-slipped, and imaged under a light microscope (Nikon, Tokyo, Japan). The percentage of TUNEL-positive cells was counted as follows: (TUNEL-positive cells)/ (total cells) × 100%.

Quantitative Real-time Polymerase Chain Reaction (qRT-PCR)

Total RNA in mice brains was extracted using the Trizol reagent (Sagon Biotech, Shanghai, China) as instructed by the manufacturer. The all-in-one cDNA Synthesis SuperMix reagent (Bimake, Shanghai, China) was used to reverse transcribe the RNA of mRNA into cDNA, based on the manufacturer's guidelines. The miRNA 1st-Strand cDNA Synthesis Kit tailing reaction reagent (Sagon Biotech, Shanghai,

China) was used to reverse transcribe the RNA of microRNA into cDNA, according to product specifications. qRT-PCR was performed using the SYBR Green qPCR Master Mix reagent (Bimake, Shanghai, China). miR-671-5p, U6, mRNA NF-κB, and β-actin expressions were evaluated using The Bio-Rad CFX Manager 3.1 system (Bio-Rad, Hercules, CA, USA). The primers used in this assay are shown in Table 1.

Cell Culture and OGD/R Treatment

Brain endothelial Bend.3 cells were cultured in Dulbecco's Modified Eagle's Medium (DMEM, Saimike, Chongqing, China) with 10% FBS (Hyclone, Logan, Utah, USA) and incubated at 37 °C in a humidified 95% air and 5% CO_2 atmosphere.

OGD/R treatment: Cells were matured in a normal complete culture medium and thereafter transferred into glucose-free DMEM (Gibco, Waltham, MA, USA) culture medium in hypoxic conditions (1.0% O_2, 93.5% N_2, 5.0% CO_2, 37 °C) for 2 h. Followed, the OGD-treated cells were cultured in a normal complete culture medium under normal conditions (95% air, 5% CO_2) for 24 h of reperfusion.

Cell Viability Assay

Cell viability was assessed using the methyl-thiazolyl diphenyl-tetrazolium bromide (MTT, Sigma, St. Louis, MO, USA) assay kit. Briefly, Bend.3 cells were seeded into 96-well plates. After cells of every group had been treated, they were supplemented with 20 μL MTT (5 mg/mL) and incubated at 37 °C for 2.5 h in the dark. Then, 150 μL of dimethyl sulfoxide (DMSO; Sigma, St. Louis, MO, USA) was added to the wells to dissolve the purple formazan crystals. The absorbance of the solvent in the wells was measured at 560 nm using a fluorescence plate reader (Thermo Fisher Scientific, Waltham, MA, USA).

Lactate Dehydrogenase (LDH) Leakage Assay

The release of cytoplasmic LDH from the intracellular environment into the cell culture medium was used to assess cell membrane integrity to inform on cell cytotoxicity. Cell cytotoxicity was evaluated using the LDH Assay Kit (Servicebio, Wuhan, China), following the manufacturer's guidelines. Absorbance intensity was measured at 490 nm using a fluorescence plate reader (Thermo Scientific, Waltham, MA, USA). LDH release (%) = LDH release of the experimental group × 100 /maximum LDH release.

Measurement of Trans-endothelial Electrical Resistance (TEER) and Fluorescein Sodium Permeability

The Bend.3 cells (3×10^4) were seeded on 24-well Transwell permeable membranes with 0.4 μm pore sizes for 7 days. After group treatments, the TEER of every group cell was measured using Millicell-ERS-2 (Millipore, USA). TEER values are shown as $\Omega \times cm^2$ based on culture inserts.

After group treatments, 100 μg/mL sodium fluorescein (Shanghai Aladdin biochemical technology, shanghai, China) was added into the top chamber of a 24-well Transwell and incubated for 30 min. The concentration of sodium fluorescein in the culture medium of the underlayer Transwell was determined at 37 °C using a fluorescence plate reader (Thermo Fisher Scientific, Waltham, MA, USA) at a 485 nm excitation and 520 nm emission. The sodium fluorescein leakage values are shown in every group /of the control group.

Western Blotting

Total proteins were extracted from mice cortex or cells by radioimmunoprecipitation assay (RIPA) lysis buffer (Dingguo, Beijing, China), separated by 10% SDS-PAGE gel fast preparation kit (Servicebio, Wuhan, China) and transferred onto polyvinylidene fluoride (PVDF) membranes (Millipore, Shanghai, China). The PVDF membranes were blocked with 5% bovine serum albumin (Thermo Fisher Scientific, Shanghai, China) for 1 h, and incubated with primary antibodies against β-actin (1:3000, Beyotime, Shanghai, China Servicebio, Wuhan, China), NF-κB (p65, 1:1000, Cell Signaling Technology, USA), MMP-9 (1:2000, Cell Signaling Technology, USA), ZO-1 (1:1000, Beyotime, Shanghai, China),

Table1 The sequence of primer for qRT-PCR

name	sequence
NF-κB	Forword: 5'-TGCGATTCCGCTATAAATGCG-3'
	Reverse: 5'-ACAAGTTCATGTGGATGAGGC-3'
β-actin	Forward:5'-GTGCTATGTTGCTCTAGACTTCG-3'
	Reverse: 5'-ATGCCACAGGATTCCATACC-3'
mmu-miR-671-5p	sense: 5'-TATAGGAAGCCCTGGAGGGG-3'
universal U6 primer	sense: 5'-CTCGCTTCGGCAGCACA-3'
	antisense: 5'-AACGCTTCACGAATT-3'

occludin (1:1000, Beyotime, Shanghai, China), claudin 5 (1:1000, Affinity Biosciences, USA, 23 kDa) at 4 °C for 24 h. Then, they were incubated with Biotin-conjugated affinipure goat anti-rabbit IgG (H + L) (1:4000, Beyotime, Shanghai, China) for 40 min. Imaging of PVDF membranes was performed using the Image Lab3.0 software (Bio-Rad, Hercules, CA, USA) after exposure by using an ECL Femto-Light Chemiluminescence Kit (Epizyme, Shanghai, China).

Immunofluorescence Staining

Every group of cells was fixed in 4% paraformaldehyde for 20 min to prepare for immunofluorescence staining. Paraffin sections were prepared from obtained mice brains. Slices and cells were dipped in 0.2% Triton X for 30 min and blocked with 5% bovine serum albumin for 2 h. Samples were then incubated at 4° C for 24 h with anti-NF-κB (1:200, Cell Signaling Technology, USA), CD31 (1:100, Servicebio, Wuhan, China), and stained with Cy3-labeled Goat Anti-Rabbit IgG (H + L) (Beyotime, Shanghai, China) as well as FITC-labeled Goat Anti-Rabbit IgG (H + L) (Beyotime, Shanghai, China). DAPI (Beyotime, Shanghai, China) was used to stain the cell nucleus. A fluorescence microscope (Nikon, Tokyo, Japan) was used for imaging. Fluorescence intensities were analyzed using ImageJ.

Statistical Analysis

Data were presented as mean ± SEM. One-way ANOVA followed by Tukey's test for multiple comparisons was performed using GraphPad Prism 6.01. Neurological score analysis was performed using the Kruskal–Wallis H test (SPSS, IBM, Chicago, IL, USA). $p < 0.05$ was the threshold for significance.

Results

miR-671-5p Levels were Suppressed in the Cortex of MCAO/R Mice

The FISH assay revealed the presence of miR-671-5p in brain microvascular endothelial cells (BMVECs), astrocytes, and neurons (Fig. 1). The expressions of miR-671-5p were suppressed in the cortex of MCAO/R mice (Fig. 2). The Kyoto Encyclopedia of Genes and Genomes (KEGG) analysis revealed that the enrichment of the NF-κB signaling pathway was higher in MCAO/R mice than in the sham group (Fig. 3A). Gene Ontology (GO) analysis of molecular functions showed that enzyme binding (GO:0019899) that included MMP-9 showed higher enrichment in MCAO/R mice than in the sham group (Fig. 3B). The miRNA-mRNA network revealed relationships between and among miR-671-5p, NF-κB, and MMP-9 (Fig. 3C).

Upregulated miR-671-5p Protects OGD/ R Bend.3 Cell Permeability

Unlike the normal controls, miR-671-5p expressions were significantly upregulated by miR-671-5p agomir ($p < 0.05$;

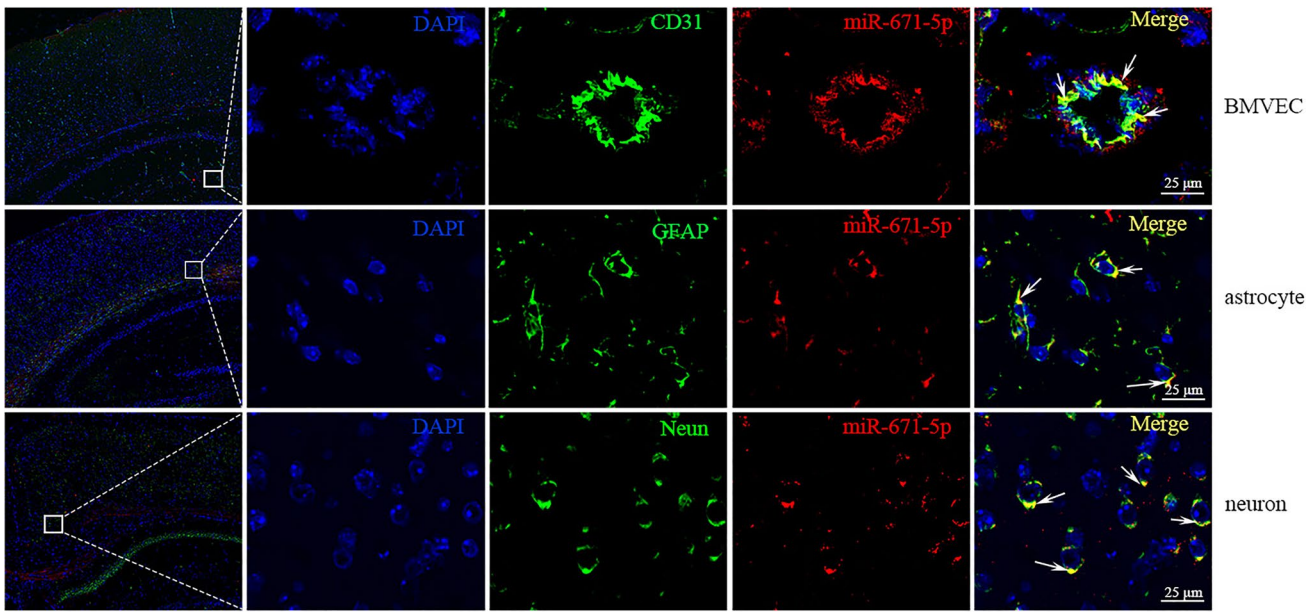

Fig. 1 The expression miR-671-5p in BBB was determined through the FISH. magnification, 400×; Blue: DAPI; green: CD31(noted brain microvessel endothelial cells (BMVEC); GFAP (noted astrocytes); Neun (noted neurons); red: miR-671-5p; yellowish: merge

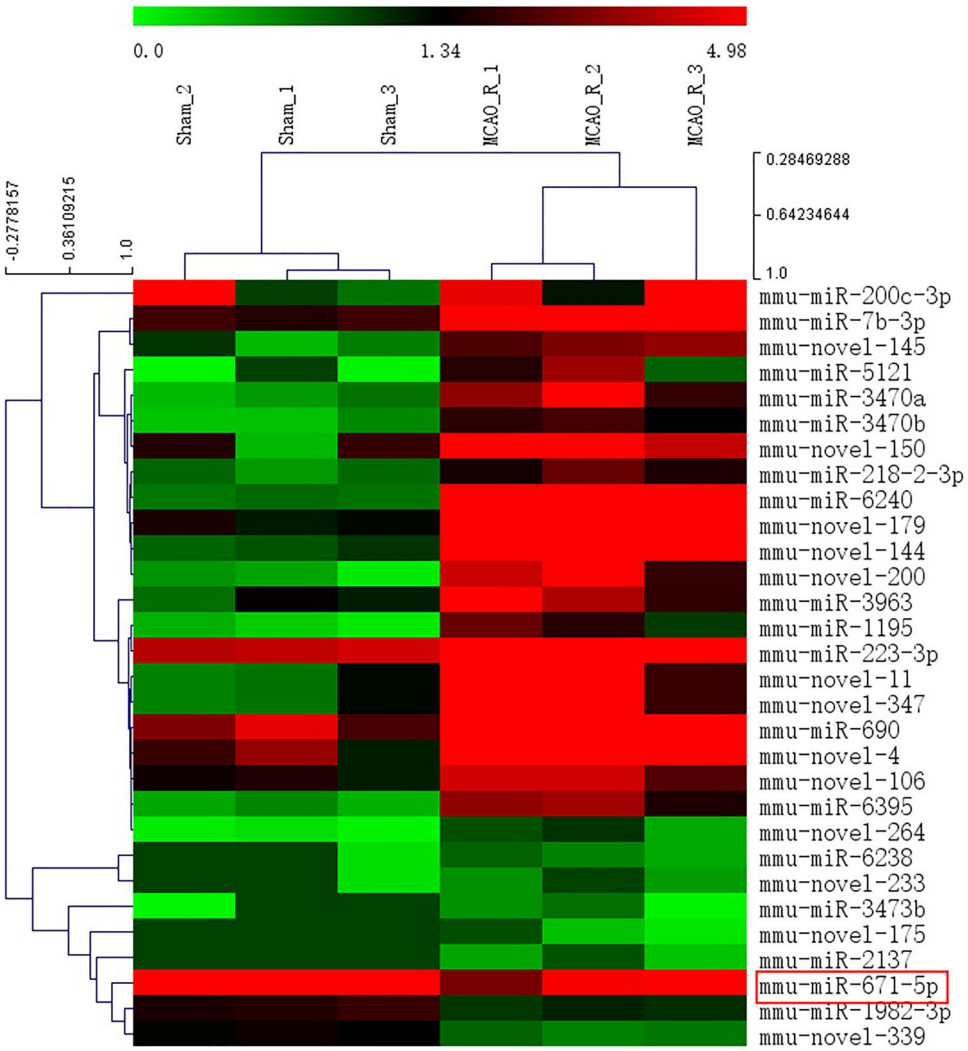

Fig. 2 Hierarchical clustering showing the top 30 downregulated or upregulated miRNAs in the MCAO/R group relative to the control group

Fig. 4A), and significantly suppressed by miR-671-5p antagomir treatments of OGD/R cells ($p < 0.05$; Fig. 4B). These findings indicated successful transfection of the miR-671-5p agomir or miR-671-5p antagomir. The viabilities of cells were lower in the OGD/R group compared to the control group ($p < 0.05$), and were increased by miR-671-5p agomir treatment ($p < 0.05$). However, miR-671-5p antagomir treatment decreased the cell viability ($p < 0.05$; Fig. 4C). Cell toxicity levels were increased in the OGD/R group compared with the control group ($p < 0.05$), but were reduced by miR-671-5p agomir treatment ($p < 0.05$; Fig. 4D). TEER level results demonstrated that the integrity of Bend.3 cells in the OGD/R group was impaired unlike that in the control group ($p < 0.05$), but was improved by miR-671-5p agomir treatment ($p < 0.05$; Fig. 4E). Fluorescein sodium permeability results revealed increased permeability of OGD/R Bend.3 cells compared to the control group ($p < 0.05$), which was reduced by miR-671-5p agomir treatment ($p < 0.05$; Fig. 4F). These results suggest that upregulated miR-671-5p protected OGD/ R Bend.3 cell permeability.

Upregulated miR-671-5p Alleviates OGD/ R Bend.3 Cell Permeability by Suppressing NF-κB Expressions

The mRNA expression of NF-κB were significantly increased in the OGD/R group, compared to that in the control group ($p < 0.05$), but were reduced by miR-671-5p agomir treatment ($p < 0.05$; Fig. 5A). Immunofluorescence analysis showed suppressed NF-κB expression in the OGD/R + miR-671-5p agomir group compared to that in the OGD/R group ($p < 0.05$; Fig. 5B, C). Therefore, upregulated miR-671-5p inhibited NF-κB expression in OGD/ R Bend.3 cells.

The mRNA expression of NF-κB was significantly increased in the OGD/R + pcDNA3.1 NF-κB group unlike that in the OGD/R group ($p < 0.05$), suggesting successful NF-κB overexpression by transfection of the pcDNA3.1- NF-κB plasmid (Fig. 5D). Treatment with the miR-671-5p agomir significantly increased the cell viabilities of OGD/R cells, which were reduced by overexpressed NF-κB (Fig. 5E). The miR-671-5p agomir

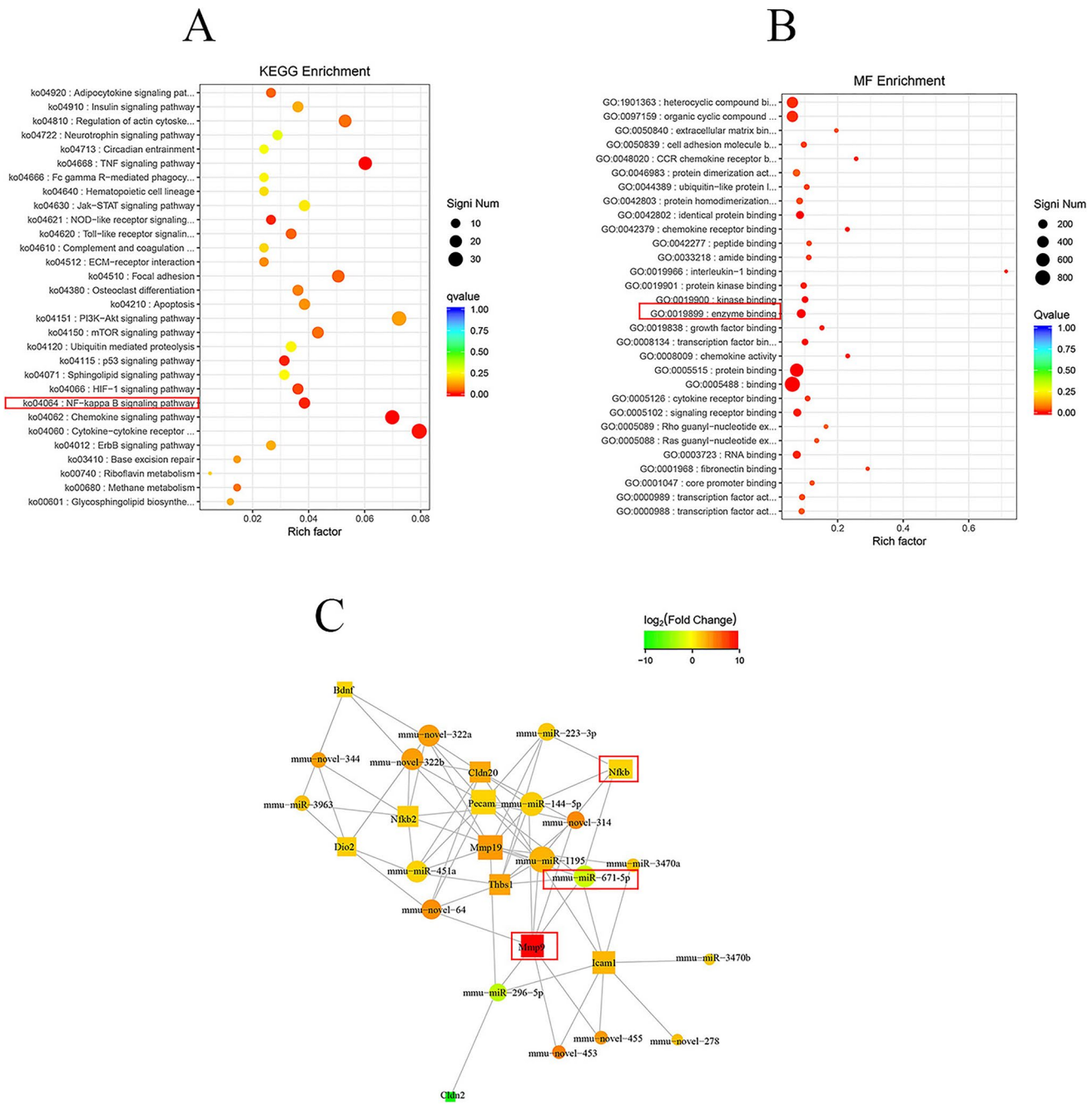

Fig. 3 Some related results of bioinformatics analysis. (**A**) Analysis of important KEGG pathways showed that the ko04064 NF-kappa B signaling pathway was enriched in MCAO/R mice. (**B**) The GO (Gene Ontology) analysis of molecular function, showed that enzyme binding (GO:0,019,899) that included MMP-9 was enriched in MCAO/R mice. (**C**) The miRNA-mRNA network. The miRNA-mRNA network revealed some relationships between and among miR-671-5p, NF-κB, and MMP-9. The circle represents miRNA, the rectangle represents mRNA, and shapes marked with different colors represent downregulated or upregulated genes

significantly reduced OGD/R cell cytotoxicity, which was reduced by overexpressed NF-κB (Fig. 5F). TEER level results demonstrated that the miR-671-5p agomir significantly improved OGD/R cell integrity, which was reduced by overexpressed NF-κB (Fig. 5G). The permeability of OGD/R cells was reduced by the miR-671-5p agomir, whereas diminished by overexpressed NF-κB (Fig. 5H). Moreover, the miR-671-5p agomir significantly suppressed the protein levels of NF-κB and MMP-9 but increased the protein levels of tight junctions (occludin, claudin 5, and ZO-1), but were reduced by overexpressed NF-κB (Fig. 5I, J).

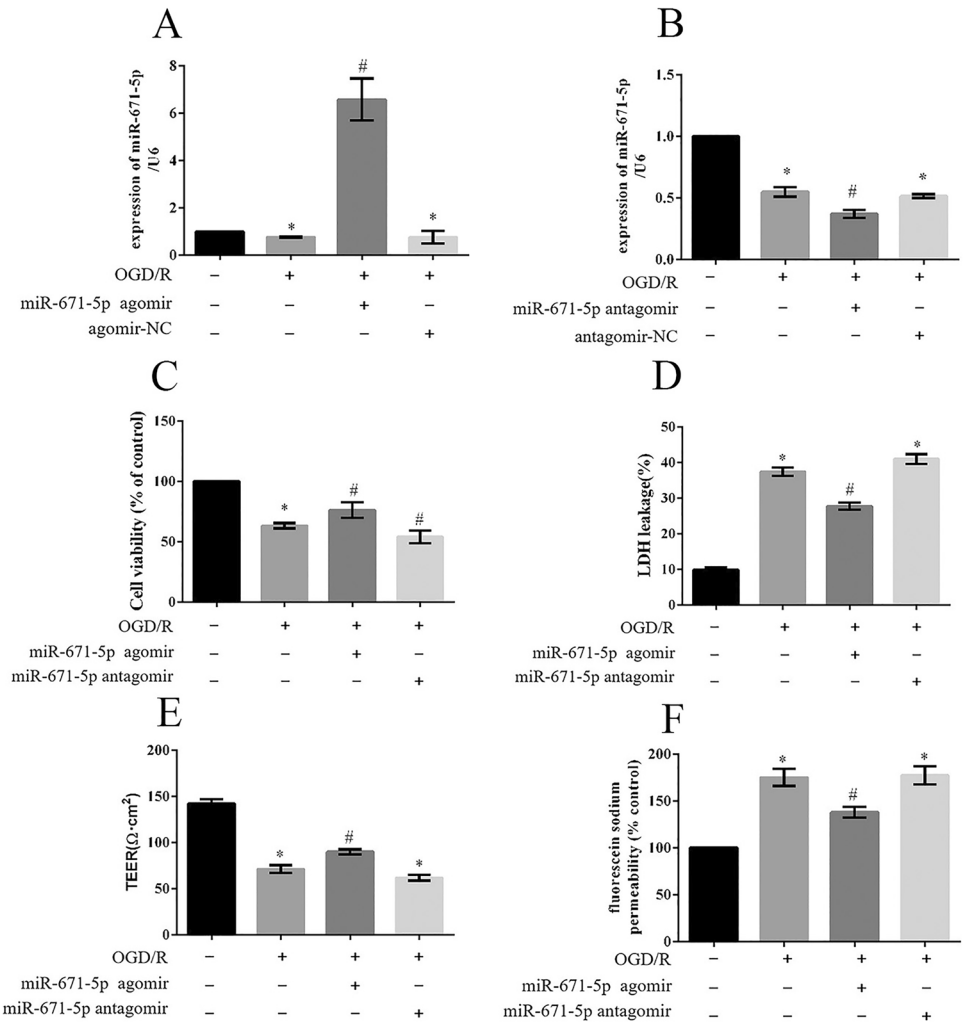

Fig. 4 The effect of miR-671-5p agomir or miR-671-5p antagomir on Bend. 3 cells were treated with OGD/R. (**A**) The expression of miR-671-5p was successfully upregulated with miR-671-5p agomir as revealed by the qRT-PCR assay. (**B**) The expression of miR-671-5p was successfully downregulated with miR-671-5p antagomir as determined by the qRT-PCR assay. (**C**) The MTT assay results show the viability of cells. (**D**) Assessment of cell injury based on lactate dehydrogenase (LDH) release rate. (**E**) TEER. (**F**) Permeability rate of fluorescein sodium. E and F The integrity and function of BBB. Values are presented as the *mean* ± *SME* from three independent experiments. Data were compared using Tukey's multiple comparisons tests followed one-way ANOVA test, * $p < 0.05$ vs control, # $p < 0.05$ vs OGD/R group

Upregulated miR-671-5p Improved BBB Permeability in MCAO/R Mice

Right intracerebroventricular injection of miR-671-5p agomir increased miR-671-5p expression compared to agomir-NC MCAO/R mice (Fig. 6A). Neurological deficit scores were higher in the MCAO/R group mice (3.6 ± 0.1), than that in the sham group (0.0 ± 0.0) ($p < 0.05$), but were significantly improved in MCAO/R mice treated with miR-671-5p agomir (1.6 ± 0.2) ($p < 0.05$; Fig. 6B). Fall latency was significantly reduced in the MCAO/R group (53.3 ± 2.0 s), compared to that in the sham controls (160.0 ± 0.0 s; $p < 0.05$), and the MCAO/R mice treated with miR-671-5p agomir remained on the Rotarod cylinder for a longer time (73.7 ± 3.8 s; $p < 0.05$; Fig. 6C). The infarcted area in the MCAO/R group mice (32.02% ± 1.70%) was significantly increased compared to that in the sham group (0.0% ± 0.0%) ($p < 0.05$), but was decreased by 14.42 ± 0.88% in MCAO/R mice treated with miR-671-5p agomir ($p < 0.05$; Fig. 6D, E). The severity of nuclear atrophy of cells treated with the miR-671-5p agomir was comparable to that of cells in the MCAO/R group. The concentration of Evans blue increased in MCAO/R mice (19.81 ± 0.78 ug/g) compared to that in the sham group (3.67 ± 0.2 ug/g; $p < 0.05$), but was reduced in MCAO/R mice treated with miR-671-5p agomir (14.16 ± 1.21 ug/g; $p < 0.05$; Fig. 6F, G). These findings indicated that upregulation of miR-671-5p protected against BBB permeability in MCAO/R mice. H&E staining showed that the proportion of injured cells in MCAO/R mice (93.36% ± 2.89%) was significantly higher than that of the sham group (7.00 ± 0.63%; $p < 0.05$), however, this proportion was reduced by 44.30 ± 4.23% in MCAO/R mice treated with miR-671-5p agomir ($p < 0.05$; Fig. 6H, I). The results of glycine silver staining showed that the axons and nerve fiber were smooth and neatly arranged in the sham group, whereas fewer axons and nerve fiber degeneration in the cortex of MCAO/R group mice compared with the sham group, which was improved by the miR-671-5p agomir therapy (Fig. 6J).

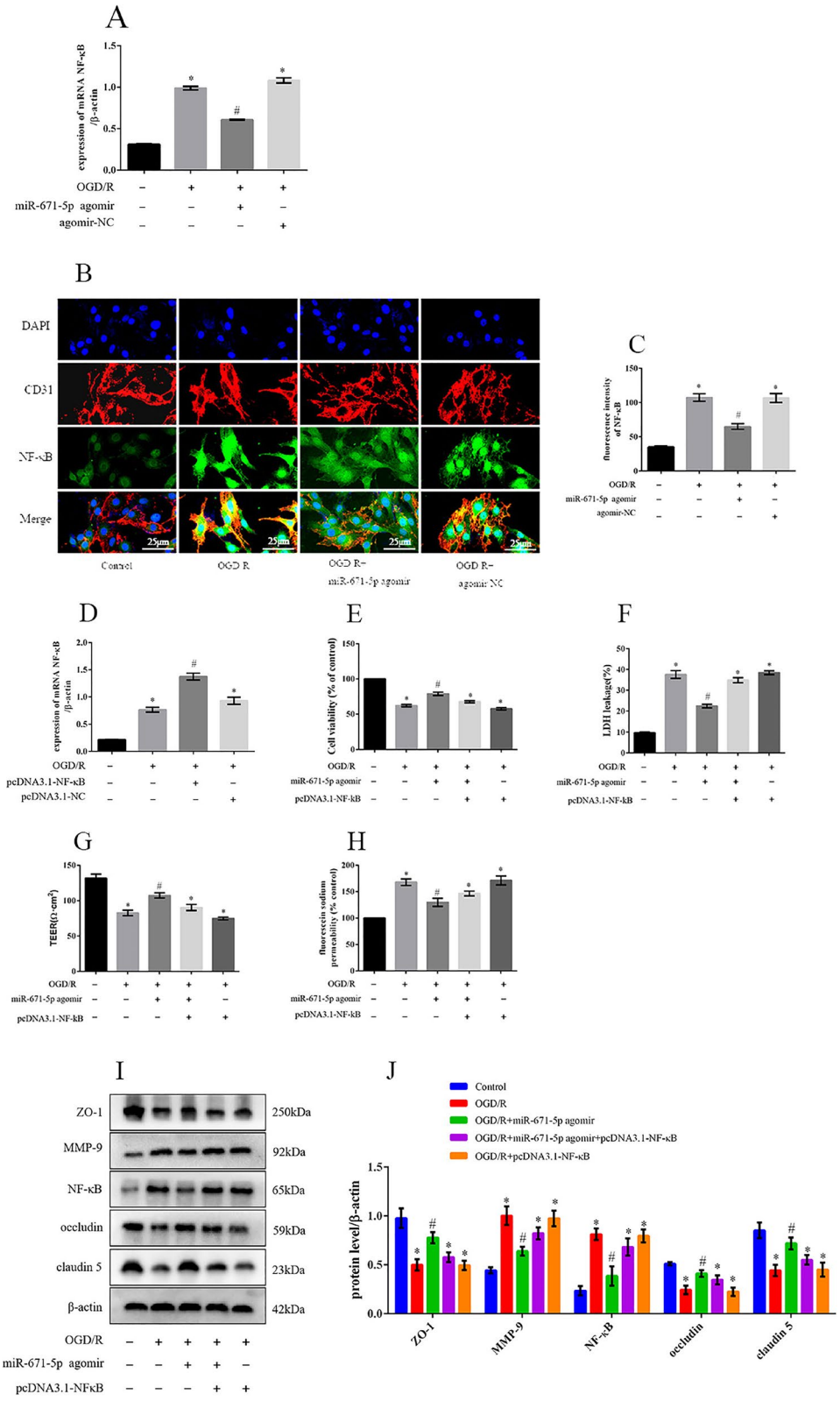

Fig. 5 Effect of miR-671-5p agomir combined with pcDNA3.1-NF-κ B on Bend.3 cells treated with OGD/R. (**A**) The miR-671-5p agomir treatment decreased mRNA NF-κB expression as revealed by qRT-PCR. (**B**, **C**) Immunofluorescent staining of NF-κB, CD31: noted BMVEC, scale bar = 250 μm. (**D**) Transfection of pcDNA3.1 NF-κB upregulated the mRNA NF-κB expression level as determined by qRT-PCR. (**E**) The MTT assay shows the viability of cells. (**F**) The lactate dehydrogenase (LDH) release rate shows the degree of cell injury. (**G**) TEER. (**H**) The permeability rate of fluorescein sodium. G and H The integrity and function of BBB. (**I**, **J**) The expression level of NF-κB, MMP-9, claudin 5, occludin, and ZO-1 was determined by western blotting. Data are presented as the *mean* ± *SME* from three independent experiments. Groups were compared using Tukey's multiple comparisons tests followed one-way ANOVA test, * $p < 0.05$ vs control, # $p < 0.05$ vs OGD/R group

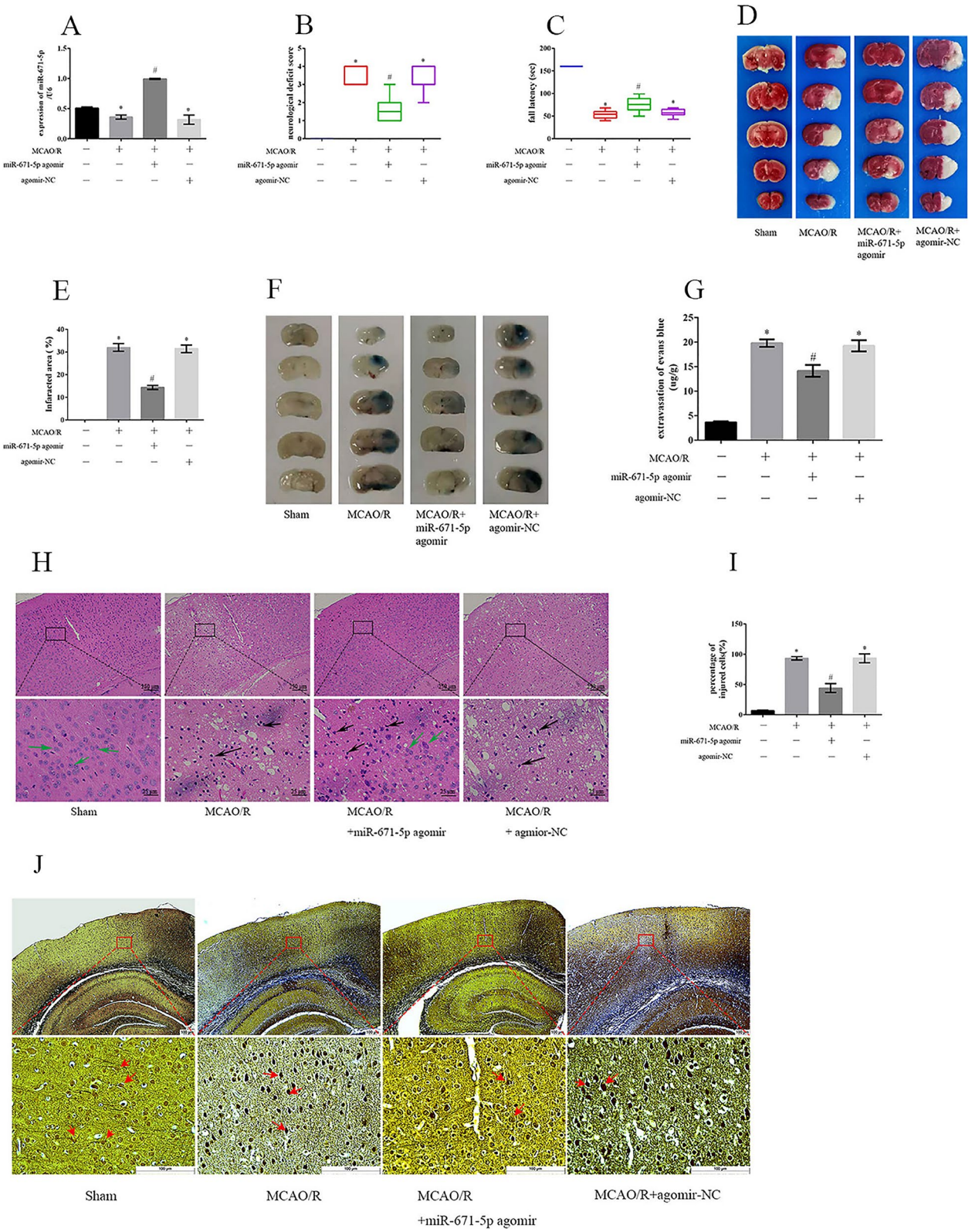
A
B
C
D
E
F
G
H
I
J
MCAO/R
miR-671-5p agomir
agomir-NC
Sham
MCAO/R
MCAO/R+ miR-671-5p agomir
MCAO/R+ agomir-NC
MCAO/R +miR-671-5p agomir
MCAO/R + agmior-NC
MCAO/R+agomir-NC

◂**Fig. 6** Impact of miR-671-5p agomir on MCAO/R mice. (**A**) The expression of miR-671-5p was successfully upregulated following miR-671-5p agomir treatment as revealed by the qRT-PCR test ($n=6$). (**B**) Neurological deficiency scores ($n=12$). (**C**) Fall latency results are based on the Rota-rod testing (sec) ($n=12$). (**D**, **E**) The cerebral infarction area was assessed through the TTC staining assay ($n=6$). (**F**, **G**) BBB permeability was evaluated using the Evans blue leakage test ($n=6$). (**H**, **I**) The H&E staining images, ($n=3$). Magnification: low-magnification: 40×, scale bar = 50 μm, high-magnification: 400×, scale bar = 250 μm; black arrow: an injured cell that nuclei shrunk, green arrow: normal cells. (**J**) The morphological changes in the cortex of mice were evaluated by glycine silver staining, the axons of neurons are pointed by the red arrows, Magnification: low-magnification: 50×, high-magnification: 400×, scale bar = 100 μm. Results are shown as *mean* ± *SEM*. Groups were analyzed using Tukey's multiple comparisons tests followed one-way ANOVA test. Kruskal–Wallis test was used to determine neurological deficit scores. *$p<0.05$ vs Sham, # $p<0.05$ vs MCAO/R group

Upregulated miR-671-5p Alleviated BBB Permeability in MCAO/R Mice by Suppressing NF-κB Expression

The mRNA expressions of NF-κB were reduced in the cortex of MCAO/R mice treated with the miR-671-5p agomir ($p<0.05$; Fig. 7A). Immunofluorescence analysis showed that NF-κB expressions in the cortex of MCAO/R mice were reduced by miR-671-5p agomir treatment (Fig. 7B, C). These findings imply that upregulated miR-671-5p suppressed NF-κB expressions in the cortex of MCAO/R mice.

The expression of NF-κB mRNA was significantly increased in the cortex of MCAO/R mice intracerebroventricularly injected with pcDNA3.1 NF-κB compared to that in the MCAO/R group ($p<0.05$), suggesting that NF-κB was successfully overexpressed in pcDNA3.1 NF-κB injected MCAO/R mice (Fig. 7D). Western blot analysis confirmed that protein levels of NF-κB and MMP-9 in the cortex of MCAO/R mice were reduced by miR-671-5p agomir treatment, however, these effects were reversed by pcDNA3.1 NF-κB. The protein levels of tight junction claudin 5, occludin and ZO-1 in the cortex of MCAO/R mice were increased by miR-671-5p agomir treatment, but these protective effects were antagonized following NF-κB overexpression (Fig. 7E, F). Apoptosis cells in the cortex increased in the MCAO/R mice (59.4 ± 1.7%) compared to that in the sham group (8.5 ± 0.8%, $p<0.05$), which were reduced by miR-671-5p agomir (35.1 ± 1.3%, $p<0.05$); however, overexpressed NF-κB reduced these protective effects by TUNEL staining (Fig. 7G, H). Neurological deficit scores were improved in the MCAO/R mice treated with the miR-671-5p agomir (1.7 ± 0.2), compared to MCAO/R group mice (3.8 ± 0.2; $p<0.05$), however, overexpressed NF-κB reduced these protective effects (Fig. 7I). Fall latency results confirmed that MCAO/R mice treated with miR-671-5p agomir could hold for a longer time (82.2 ± 2.7 s), compared to MCAO/R mice (56.2 ± 2.7 s; $p<0.05$) (Fig. 7J), however, These results suggest that upregulated miR-671-5p alleviated BBB permeability in MCAO/R mice by suppressing NF-κB expression. overexpressed NF-κB reduced these protective effects.

Discussion

The blood-brain barrier (BBB) is a structure comprising cerebral microvascular endothelial cells, pericytes, astrocytic endfeet, neurons, extracellular matrix, and tight junctions between endothelial cells that maintain the microenvironmental homeostasis of the cerebral [28, 29]. BBB destruction induced by ischemia/reperfusion may potentially trigger secondary brain injuries, including inflammation, edema, and hemorrhagic transformation [6, 30, 31]. BBB protection prevents secondary brain injury following ischemia/reperfusion. Maintaining BBB integrity and reducing BBB permeability may be an effective strategy to prevent brain damage. This study provides a novel insight into the role of miR-671-5p in the attenuation of BBB damage by suppressing NF-κB/MMP-9 to maintain BBB integrity after ischemia/reperfusion.

The FISH assay revealed the expressions of miR-671-5p in microvascular endothelial cells (BMVEC), astrocytes, and neurons, suggesting its abundance in BBB (Fig. 1). We found that miR-671-5p levels were suppressed in the cortex of MCAO/R mice by hierarchical clustering (Fig. 2). We also confirmed the downregulation of miR-671-5p both in the cortex of MCAO/R mice (Fig. 6A) and in OGD/R Bend.3 brain endothelial cells (Fig. 4A) by RT-PCR. These findings imply miR-671-5p downregulation both in vivo and in vitro ischemia/reperfusion model.

Microvascular endothelial cells were the primary cells that constitute the blood-brain barrier, Bend.3 brain endothelial cells were used to construct *in vitro* model. Upregulation of miR-671-5p *in vitro* by transfering miR-671-5p agomir reduced cells cytotoxicity, improved cell viability, and transendothelial electrical resistance, and reduced fluorescein sodium permeability of OGD/R Bend. 3 cells. However, miR-671-5p downregulation by transfection of miR-671-5p antagomir did not induce significant protective effects on OGD/R Bend.3 cells. The miR-671-5p agomir reduced BBB permeability *in vivo*, improved neurobehavioral function injury, and motor balance capacity reduced infarcted area, as well as lessened cell injury and apoptosis in the brain of MCAO/R mice. These findings imply that miR-671-5p upregulation protects against BBB destruction induced by ischemia/reperfusion.

Furthermore, we investigated the molecular mechanisms underlying the protective effects of miR-671-5p agomir. The nuclear factor kappa B (NF-κB) pathways mediate IS development by regulating the transcriptional expression of target genes or activities of other pathways,

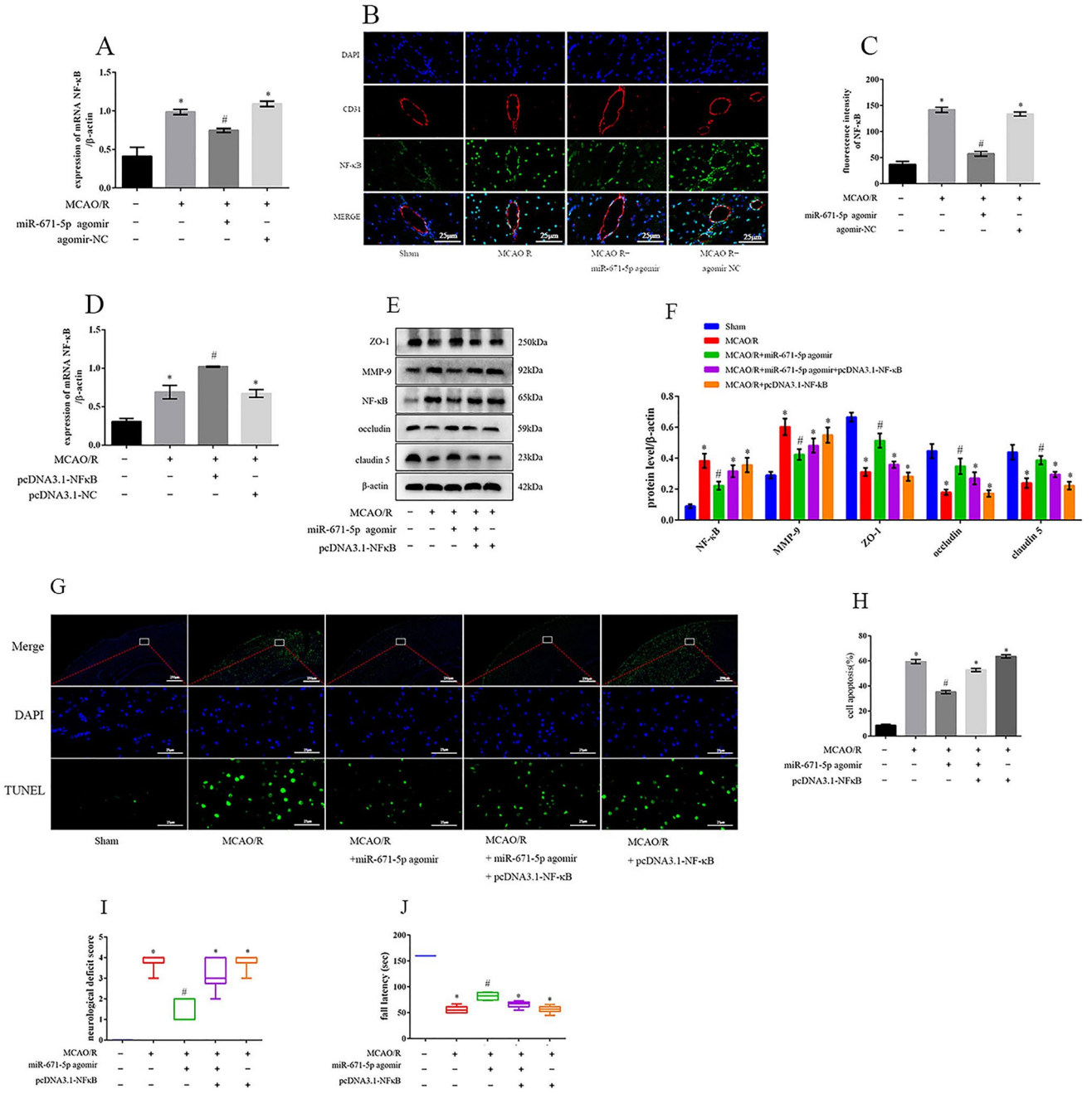

Fig. 7 Effect of miR-671-5p agomir combined with pcDNA3.1-NF-κB on the cortex of MCAO/R mice. (**A**) Treatment with miR-671-5p agomir decreased mRNA NF-κB expression level as determined by qRT-PCR ($n=6$). (**B**, **C**) Immunofluorescent staining of NF-κB and CD31: noted BMVEC ($n=3$). (**D**) mRNA Transfection with pcDNA3.1 NF-κB upregulated NF-κB expression as revealed by qRT-PCR, ($n=6$). (**E**, **F**) The relative protein levels of NF-κB, MMP-9, claudin 5, occludin, and ZO-1 were analyzed by western blotting ($n=6$). (**G**, **H**) Apoptosis cells in the cortex were analyzed by TUNEL ($n=6$). Magnification: low-magnification: 40×, scale bar = 50 μm, high-magnification: 400×, scale bar = 250 μm. (**I**) Neurological deficit scores ($n=6$). (**J**) Fall latency results as assessed by the Rota-rod test (sec) ($n=6$). Data are shown as the *mean* ± *SEM*. Groups were analyzed by Tukey's multiple comparisons tests followed one-way ANOVA test. Neurological deficit scores were determined by the Kruskal–Wallis test. *$p<0.05$ vs Sham, # $p<0.05$ vs MCAO/R group

thereby causing inflammation that aggravates BBB disruption [32]. Consequently, we noted that overexpressed NF-κB reversed the protective effects of miR-671-5p agomir in IS models. In our previous study, we found that NF-κB is a target of miR-671-5p [21]. These findings suggest that upregulation of miR-671-5p protects against BBB destruction by inhibiting NF-κB in ischemia stroke models.

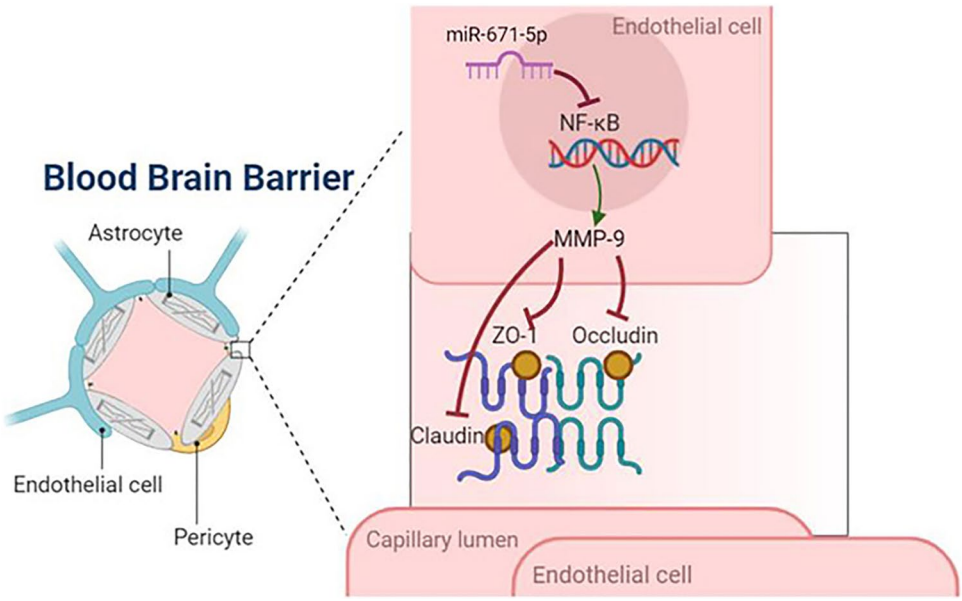

Fig. 8 The miR-671-5p/NF-κB/MMP-9/occludin pathway after ischemic stroke injury. (This figure was drawn on https://app.biorender.com/illustrations.) In the ischemic stroke model, miR-671-5p levels in the cortex were increased and upregulated miR-671-5p reduced the tight junctions of BBB by negatively regulating NF-κB/MMP-9

Matrix metallopeptidases (MMPs) are a family of zinc endopeptidases that can degrade extracellular matrix and basement membrane components [33]. Increased MMP-2 and MMP-9 levels in ischemia/reperfusion correlate with degradation of the integrity of the BBB [17, 34]. After ischemic stroke, MMP-9 is upregulated and activated, which dysregulates BBB integrity by degrading tight junction proteins and modulating inflammation [29, 35]. Tight junction proteins between endothelial cells act as gatekeepers to regulate substances entering the brain, thereby maintaining microenvironmental homeostasis of the cerebra [35, 36]. After IS, BBB disruption is accompanied by the degradation of tight junction proteins, causing edema and hemorrhagic transformation [17, 37]. Occludin, Claudins, and Zonula occludens (ZO-1, ZO-2, ZO-3) are the major members of tight junction proteins. MMP-9 suppression alleviates occludin and ZO-1 degradation in focal cerebral ischemia [7, 38], and NF-κB is one of the key transcription factors that cause MMP-9 expression [39–41].

MMP-9 is highly abundant in the hippocampus, cerebellum, and cerebral cortex regions of the brain [42]. In this work, samples from the cerebral cortex of MCAO/R mice, and the miRNA-mRNA network demonstrated relationships between miR-671-5p, NF-κB, and MMP-9.

Our findings revealed that upregulated miR-671-5p suppressed MMP-9 expressions and increased occludin, claudins, and ZO-1 levels, which were reversed by overexpressed NF-κB both in Bend.3 OGD/R cells (Fig. 5) and in the cortex of MCAO/R mice (Fig. 7). In summary, these findings show that upregulated miR-671-5p alleviates tight junction protein permeability of BBB by suppressing NF-κB, thereby inhibiting MMP-9 expressions induced by ischemia/reperfusion.

This study has compelling limitations. The NF-κB transcription factor comprises homodimers or heterodimers of p50, p52, p65, Rela-B, and c-Rel proteins. The p65 protein is important for NF-κB functionality, and the p65 represents NF-κB in Western blot assay. miR-671-5p is an RNA nucleotide sequence that can directly regulate NF-κB expressions only at mRNA levels via transcription or translation, thus, it can regulate *de novo* ischemia/reperfusion-induced NF-κB transcription or translation. One of the steps of translation is modulated by cytoplasmic ribosomes, therefore, we measured the total NF-κB levels in whole cells of samples without analyzing differences in the cytoplasm or nucleus. Since miR-671-5p expression was not significantly changed following agomir-NC treatment *in vitro* Fig. 4 and in vivo Fig. 6, we did not design the agomir-NC group in Fig. 5 and Fig. 7.

Conclusion

In conclusion, miR-671-5p levels were inhibited, and upregulated miR-671-5p alleviated BBB permeability by suppressing NF-κB/MMP-9 in both *in vitro and in vivo* ischemia/reperfusion model (Fig. 8). These findings suggest that miR-671-5p is a potential biomarker and therapeutic target that maintains BBB permeability during IS. Nonetheless, the safety, efficacy, and mechanism of miR-671-5p in IS patients warrant further investigations.

Supplementary Information The online version contains supplementary material available at https://doi.org/10.1007/s12035-023-03318-7.

Acknowledgements This study was supported by funds from the Science and Technology Bureau of Yuzhong in Chongqing, Chongqing Science and Technology Bureau, and Chongqing Health Commission.

Author Contribution Ling Deng participated in the conceptualization, design of methodology, writing, and editing the manuscript. Jiyu Zhang and Sha Chen contributed to the conceptualization, writing, reviewing, & editing the manuscript. Yu Wu, Xiaomei Fan, Tianrui Zuo, Qingwen Hu, Lu Jiang, and Shaolan Yang designed the methodology and performed experiments. Zhi Dong provided funding acquisition and administrated the project. All authors read and approved the final manuscript.

Funding This study was partially supported by the General Topics of Basic Research and Frontier Exploration of Yuzhong district, Chongqing (20210121); Medical Research Project of Chongqing Science and Technology Bureau and Chongqing Health Commission (2022QNXM068); Postdoctoral Science Foundation of Chongqing (CSTB2022NSCQ-BHX0.684).

Data Availability All data generated or analyzed during this study are available from the corresponding author's email.

Declarations

Ethics Approval This article does not contain any studies with human participants performed by any of the authors. All animal procedures were approved by the Ethical Committee of Chongqing Medical University. The authors have no ethical conflicts to disclose.

Consent for Publication Not applicable.

Consent to Participate Not applicable.

Competing Interests The authors declare that they have no competing interests.

References

1. Mendelson SJ, Prabhakaran S (2021) Diagnosis and Management of Transient Ischemic Attack and Acute Ischemic Stroke: A Review. JAMA 325(11):1088–1098. https://doi.org/10.1001/jama.2020.26867
2. Campbell BCV, Khatri P (2020) Stroke. Lancet 396(10244):129–142. https://doi.org/10.1016/S0140-6736(20)31179-X
3. Phipps MS, Cronin CA (2020) Management of acute ischemic stroke. BMJ 368:l6983. https://doi.org/10.1136/bmj.l6983
4. Feske SK (2021) Ischemic Stroke. Am J Med 134(12):1457–1464. https://doi.org/10.1016/j.amjmed.2021.07.027
5. Ronaldson PT, Davis TP (2020) Regulation of blood-brain barrier integrity by microglia in health and disease. A therapeutic opportunity J Cereb Blood Flow Metab 40(1_suppl):6–24. https://doi.org/10.1177/0271678X20951995
6. Abdullahi W, Tripathi D, Ronaldson PT (2018) Blood-brain barrier dysfunction in ischemic stroke: targeting tight junctions and transporters for vascular protection. Am J Physiol Cell Physiol 315(3):C343–C356. https://doi.org/10.1152/ajpcell.00095.2018
7. Saleem S, Wang D, Zhao T, Sullivan RD, Reed GL (2021) Matrix Metalloproteinase-9 Expression is Enhanced by Ischemia and Tissue Plasminogen Activator and Induces Hemorrhage, Disability and Mortality in Experimental Stroke. Neuroscience 460:120–129. https://doi.org/10.1016/j.neuroscience.2021.01.003
8. Eyileten C, Wicik Z, De Rosa S, Mirowska-Guzel D, Soplinska A, Indolfi C, Jastrzebska-Kurkowska I, Czlonkowska A et al (2018) MicroRNAs as Diagnostic and Prognostic Biomarkers in Ischemic Stroke-A Comprehensive Review and Bioinformatic Analysis. Cells 7(12):249. https://doi.org/10.3390/cells7120249
9. Rupaimoole R, Slack FJ (2017) MicroRNA therapeutics: towards a new era for the management of cancer and other diseases. Nat Rev Drug Discov 16(3):203–222. https://doi.org/10.1038/nrd.2016.246
10. Qian Y, Chopp M, Chen J (2020) Emerging role of microRNAs in ischemic stroke with comorbidities. Exp Neurol 331:113382. https://doi.org/10.1016/j.expneurol.2020.113382
11. Eyileten C, Sharif L, Wicik Z, Jakubik D, Jarosz-Popek J, Soplinska A, Postula M, Czlonkowska A et al (2021) The Relation of the Brain-Derived Neurotrophic Factor with MicroRNAs in Neurodegenerative Diseases and Ischemic Stroke. Mol Neurobiol 58(1):329–347. https://doi.org/10.1007/s12035-020-02101-2
12. Zhang X, Hamblin MH, Yin K-J (2019) Noncoding RNAs and Stroke. Neuroscientist 25(1):22–26. https://doi.org/10.1177/1073858418769556
13. Piwecka M, Glažar P, Hernandez-Miranda LR, Memczak S, Wolf SA, Rybak-Wolf A, Filipchyk A, Klironomos F et al (2017) Loss of a mammalian circular RNA locus causes miRNA deregulation and affects brain function. Science 357(6357):eaam8526. https://doi.org/10.1126/science.aam8526
14. Kleaveland B, Shi CY, Stefano J, Bartel DP (2018) A Network of Noncoding Regulatory RNAs Acts in the Mammalian Brain. Cell 174(2):350-362.e17. https://doi.org/10.1016/j.cell.2018.05.022
15. Ma C, Nie Z-K, Guo H-M, Kong Y (2020) MiR-671–5p plays a promising role in restraining osteosarcoma cell characteristics through targeting TUFT1. J Biochem Mol Toxicol 34(7):e22490. https://doi.org/10.1002/jbt.22490
16. Lin J-C, Kuo C-Y, Tsai J-T, Liu W-H (2021) miR-671–5p Inhibition by MSI1 Promotes Glioblastoma Tumorigenesis via Radioresistance, Tumor Motility and Cancer Stem-like Cell Properties. Biomedicines 10(1):21. https://doi.org/10.3390/biomedicines10010021
17. Yang C, Hawkins KE, Doré S, Candelario-Jalil E (2019) Neuroinflammatory mechanisms of blood-brain barrier damage in ischemic stroke. Am J Physiol Cell Physiol 316(2):C135–C153. https://doi.org/10.1152/ajpcell.00136.2018
18. Zhang S, An Q, Wang T, Gao S, Zhou G (2018) Autophagy- and MMP-2/9-mediated Reduction and Redistribution of ZO-1 Contribute to Hyperglycemia-increased Blood-Brain Barrier Permeability During Early Reperfusion in Stroke. Neuroscience 377:126–137. https://doi.org/10.1016/j.neuroscience.2018.02.035
19. Mohamed HA, Said RS (2021) Coenzyme Q10 attenuates inflammation and fibrosis implicated in radiation enteropathy through suppression of NF-kB/TGF-β/MMP-9 pathways. Int Immunopharmacol 92:107347. https://doi.org/10.1016/j.intimp.2020.107347
20. Ha S-H, Kwon K-M, Park J-Y, Abekura F, Lee Y-C, Chung T-W, Ha K-T, Chang HW et al (2019) Esculentoside H inhibits colon cancer cell migration and growth through suppression of MMP-9 gene expression via NF-kB signaling pathway. J Cell Biochem 120(6):9810–9819. https://doi.org/10.1002/jcb.28261
21. Deng L, Guo Y, Liu J, Wang X, Chen S, Wang Q, Rao J, Wang Y et al (2021) miR-671-5p Attenuates Neuroinflammation via Suppressing NF-κB Expression in an Acute Ischemic Stroke Model. Neurochem Res 46(7):1801–1813. https://doi.org/10.1007/s11064-021-03321-1
22. Liu H, Zhao M-J, Wang Z-Y, Han Q-Q, Wu H-Y, Mao X-F, Wang Y-X (2019) Involvement of d-amino acid oxidase in cerebral ischaemia induced by transient occlusion of the middle cerebral artery in mice. Br J Pharmacol 176(17):3336–3349. https://doi.org/10.1111/bph.14764

23. Li F, Xu D, Hou K, Gou X, Lv N, Fang W, Li Y (2021) Pretreatment of Indobufen and Aspirin and their Combinations with Clopidogrel or Ticagrelor Alleviates Inflammasome Mediated Pyroptosis Via Inhibiting NF-κB/NLRP3 Pathway in Ischemic Stroke. J Neuroimmune Pharmacol 16(4):835–853. https://doi.org/10.1007/s11481-020-09978-9
24. Hayashi K, Hasegawa Y, Takemoto Y, Cao C, Takeya H, Komohara Y, Mukasa A, Kim-Mitsuyama S (2019) Continuous intracerebroventricular injection of Porphyromonas gingivalis lipopolysaccharide induces systemic organ dysfunction in a mouse model of Alzheimer's disease. Exp Gerontol 120:1–5. https://doi.org/10.1016/j.exger.2019.02.007
25. Ji Y, Teng L, Zhang R, Sun J, Guo Y (2017) NRG-1β exerts neuroprotective effects against ischemia reperfusion-induced injury in rats through the JNK signaling pathway. Neuroscience 362:13–24. https://doi.org/10.1016/j.neuroscience.2017.08.032
26. Wang C, Jiang Q, Zhao P (2022) Sevoflurane exposure during the second trimester induces neurotoxicity in offspring rats by hyperactivation of PARP-1. Psychopharmacology 239(9):3031–3045. https://doi.org/10.1007/s00213-022-06188-4
27. Ding Y-X, Eerduna G-W, Duan S-J, Li T, Liu R-X, Zhang L-M, Wang T, Fu F-H (2021) Escin ameliorates the impairments of neurological function and blood brain barrier by inhibiting systemic inflammation in intracerebral hemorrhagic mice. Exp Neurol 337:113554. https://doi.org/10.1016/j.expneurol.2020.113554
28. Xu S-Y, Bian H-J, Shu S, Xia S-N, Gu Y, Zhang M-J, Xu Y, Cao X (2021) AIM2 deletion enhances blood-brain barrier integrity in experimental ischemic stroke. CNS Neurosci Ther 27(10):1224–1237. https://doi.org/10.1111/cns.13699
29. Qi Z, Liang J, Pan R, Dong W, Shen J, Yang Y, Zhao Y, Shi W et al (2016) Zinc contributes to acute cerebral ischemia-induced blood-brain barrier disruption. Neurobiol Dis 95:12–21. https://doi.org/10.1016/j.nbd.2016.07.003
30. Ng FC, Churilov L, Yassi N, Kleinig TJ, Thijs V, Wu TY, Shah DG, Dewey HM et al (2021) Microvascular Dysfunction in Blood-Brain Barrier Disruption and Hypoperfusion Within the Infarct Posttreatment Are Associated With Cerebral Edema. Stroke 53(5):1579-1605. https://doi.org/10.1161/STROKEAHA.121.036104
31. D'Souza A, Dave KM, Stetler RA, Manickam DS (2021) Targeting the blood-brain barrier for the delivery of stroke therapies. Adv Drug Deliv Rev 171:332–351. https://doi.org/10.1016/j.addr.2021.01.015
32. Arumugam TV, Baik S-H, Balaganapathy P, Sobey CG, Mattson MP, Jo D-G (2018) Notch signaling and neuronal death in stroke. Prog Neurobiol 165–167:103–116. https://doi.org/10.1016/j.pneurobio.2018.03.002
33. Walter L, Canup B, Pujada A, Bui TA, Arbasi B, Laroui H, Merlin D, Garg P (2020) Matrix metalloproteinase 9 (MMP9) limits reactive oxygen species (ROS) accumulation and DNA damage in colitis-associated cancer. Cell Death Dis 11(9):767. https://doi.org/10.1038/s41419-020-02959-z
34. Zeng C, Wang D, Chen C, Chen L, Chen B, Li L, Chen M, Xing H (2020) Zafirlukast protects blood-brain barrier integrity from ischemic brain injury. Chem Biol Interact 316:108915. https://doi.org/10.1016/j.cbi.2019.108915
35. Liao B, Geng L, Zhang F, Shu L, Wei L, Yeung PKK, Lam KSL, Chung SK et al (2020) Adipocyte fatty acid-binding protein exacerbates cerebral ischaemia injury by disrupting the blood-brain barrier. Eur Heart J 41(33):3169–3180. https://doi.org/10.1093/eurheartj/ehaa207
36. Bauer AT, Bürgers HF, Rabie T, Marti HH (2010) Matrix metalloproteinase-9 mediates hypoxia-induced vascular leakage in the brain via tight junction rearrangement. J Cereb Blood Flow Metab 30(4):837–848. https://doi.org/10.1038/jcbfm.2009.248
37. Jiang X, Andjelkovic AV, Zhu L, Yang T, Bennett MVL, Chen J, Keep RF, Shi Y (2018) Blood-brain barrier dysfunction and recovery after ischemic stroke. Prog Neurobiol 163–164:144–171. https://doi.org/10.1016/j.pneurobio.2017.10.001
38. Liu W, Hendren J, Qin X-J, Shen J, Liu KJ (2009) Normobaric hyperoxia attenuates early blood-brain barrier disruption by inhibiting MMP-9-mediated occludin degradation in focal cerebral ischemia. J Neurochem 108(3):811–820. https://doi.org/10.1111/j.1471-4159.2008.05821.x
39. Pan Y, Zhang Y, Yuan J, Ma X, Zhao Y, Li Y, Li F, Gong X et al (2020) Tetrahydrocurcumin mitigates acute hypobaric hypoxia-induced cerebral oedema and inflammation through the NF-κB/VEGF/MMP-9 pathway. Phytother Res 34(11):2963–2977. https://doi.org/10.1002/ptr.6724
40. Zhang L, Graf I, Kuang Y, Zheng X, Haupt M, Majid A, Kilic E, Hermann DM et al (2021) Neural Progenitor Cell-Derived Extracellular Vesicles Enhance Blood-Brain Barrier Integrity by NF-κB (Nuclear Factor-κB)-Dependent Regulation of ABCB1 (ATP-Binding Cassette Transporter B1) in Stroke Mice. Arterioscler Thromb Vasc Biol 41(3):1127–1145. https://doi.org/10.1161/ATVBAHA.120.315031
41. Bell RD, Winkler EA, Singh I, Sagare AP, Deane R, Wu Z, Holtzman DM, Betsholtz C et al (2012) Apolipoprotein E controls cerebrovascular integrity via cyclophilin A. Nature 485(7399):512–516. https://doi.org/10.1038/nature11087
42. Mondal S, Adhikari N, Banerjee S, Amin SA, Jha T (2020) Matrix metalloproteinase-9 (MMP-9) and its inhibitors in cancer: A minireview. Eur J Med Chem 194:112260. https://doi.org/10.1016/j.ejmech.2020.112260